iScience

CellPress
OPEN ACCESS

Article

Facile All-Optical Method for *In Situ* Detection of Low Amounts of Ammonia

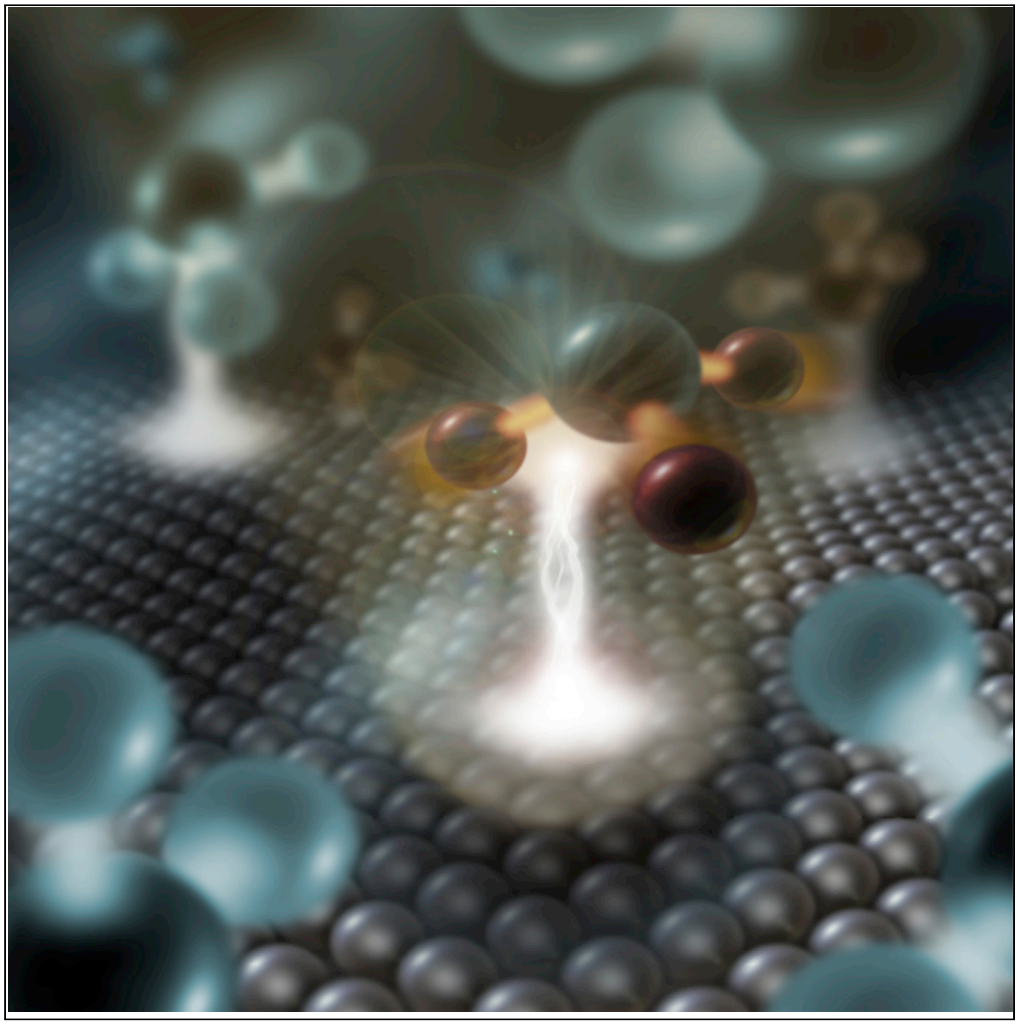

Yuanchao Liu, Tristan Asset, Yechuan Chen, ..., Ivana Matanovic, Dmitry A. Fishman, Plamen Atanassov

dmitryf@uci.edu

HIGHLIGHTS

Novel method for detection of ammonia at concentrations below 1 ppm in just under 1 s

This approach allows local detection of ammonia amounts as low as 10^4–10^5 molecules

Method for sensitive direct monitoring of catalytic/electrocatalytic processes

The method allows following the dynamics of ammonia concentration change in real time

Liu et al., iScience *23*, 101757
November 20, 2020
https://doi.org/10.1016/j.isci.2020.101757

iScience

CellPress
OPEN ACCESS

Article

Facile All-Optical Method for *In Situ* Detection of Low Amounts of Ammonia

Yuanchao Liu,[1] Tristan Asset,[1] Yechuan Chen,[1] Eamonn Murphy,[1] Eric O. Potma,[2] Ivana Matanovic,[3] Dmitry A. Fishman,[2,4,5,*] and Plamen Atanassov[1,4]

SUMMARY

As a key precursor for nitrogenous compounds and fertilizer, ammonia affects our lives in numerous ways. Rapid and sensitive detection of ammonia is essential, both in environmental monitoring and in process control for industrial production. Here we report a novel and nonperturbative method that allows rapid detection of ammonia at low concentrations, based on the all-optical detection of surface-enhanced Raman signals. We show that this simple and affordable approach enables ammonia probing at selected regions of interest with high spatial resolution, making *in situ* and *operando* observations possible.

INTRODUCTION

Ammonia is key to many chemical technologies that drive world economies (Haber, 1905; Bosch, 1908), being the major source for fertilizers for agriculture/food production (Ampuero and Bosset, 2003) and directly used in multitude of industrial processes (Chen et al., 2018). Ammonia analyses are critical for water quality control (Baird and Bridgewater, 1995), exhaust gas sensing (Docquier and Candel, 2002; Riegel et al., 2002), monitoring and process control in industries of new chemicals, plastics, and pharmaceutical. It is also critical in detection of combustibles (Kohl, 2001), detonation, and propulsion processes. Moreover, it is at heart of our quest to find alternative routes of nitrogen fixation mechanisms for large-scale ammonia generation that are more efficient, energy saving, and carbon dioxide footprint free (Andersen et al., 2019; Tang and Qiao, 2019; Qing et al., 2020; Cui et al., 2018). In all of these processes, rapid and sensitive detection of ammonia is critical, thus driving a need for reliable ammonia sensing technologies. Current detection concepts are based on various "wet chemistry" processes and devices—electrochemical sensor devices (Chang et al., 1993; Lundström et al., 1993; Timmer et al., 2005), metal oxides (Clifford and Tuma, 1982; Hübner and Drost, 1991; Imawan et al., 2000; Srivastava et al., 1994; Wang et al., 2000; Xu et al., 2000; Yamazoe, 1991; Zakrzewska, 2001), catalytic polymer (Cai et al., 2001; Chabukswar et al., 2001; Heiduschka et al., 1997; Kukla et al., 1996; Lähdesmäki et al., 1996, 2000; Nicolas-Debarnot and Poncin-Epaillard, 2003; Palmqvist et al., 1995), inkjet printing films (Lv et al., 2019), polymer hybrid framework (Ahmadi Tabr et al., 2019). Spectroscopic methods for ammonia detection include nuclear magnetic resonance (NMR) (Nielander et al., 2019; Andersen et al., 2019) and optical spectroscopy in almost every part of electro-magnetic spectrum, ranging from the UV (Mount et al., 2002) to the far IR branch (Giovannozzi et al., 2015; Max and Chapados, 2013; Patton and Crouch, 1977; Tzollas et al., 2010; Li and Keppler, 2014; Ujike and Tominaga, 2002), optoelectronic (Zilberman et al., 2014; Mahendran and Philip, 2013) and specially designed fiber sensors (Guo and Tao, 2007).

Among the full arsenal of ammonia detection methods (Timmer et al., 2005), spectroscopic approaches are of particular interest as they provide direct information on chemical content and unambiguously identify the presence of the target molecular compound even at low concentrations. Traditionally, NMR spectroscopy has been the method of choice for sensitive ammonia detection (Nielander et al., 2019; Andersen et al., 2019). NMR provides chemical selectivity and high sensitivity down to 3 μM of the target and is rightfully among the most trusted approaches. However, complex instrumentation and large required sampling volumes (>0.5 mL) constitute serious limitations. More importantly, sensitive to contamination, the NMR approach relies on using isotope labeling, which renders even routine experiments very expensive and limits applications mainly to fundamental research in laboratory environments.

[1]Department of Chemical & Biomolecular Engineering, National Fuel Cell Research Center (NFCRC), University of California, Irvine, CA 92697, USA

[2]Department of Chemistry, University of California, Irvine, CA 92697, USA

[3]Department of Chemical and Biological Engineering, University of New Mexico, Albuquerque, NM 87131, USA

[4]These authors contributed equally

[5]Lead Contact

*Correspondence: dmitryf@uci.edu

https://doi.org/10.1016/j.isci.2020.101757

At present, the most popular and widely adopted optical methods are based on colorimetric approaches and their experimental derivatives (Searle, 1984). A popular solution employs the Berthelot reaction between ammonia, chlorine, and phenolic compounds, resulting in blue coloration of an indophenol dye that can be easily detected by conventional spectrometers (Patton and Crouch, 1977). This approach allows ammonia detection with an impressive sensitivity, down to several tens of ppb (parts per billion) (Bolleter et al., 1961; Patton and Crouch, 1977; Tzollas et al., 2010; Zhao et al., 2019). Although considered as the "gold standard," the blue indophenol method requires time-consuming sample handling. An aliquot of >1 mL has to be collected from the chemical reactor and mixed with toxic, sample-altering reagents, followed by tens of minutes of aging prior to spectroscopic analysis.

In this context, the availability of a detection method for ammonia and its derivatives that is robust, affordable, and universally applicable would be highly desirable. We envision that *simplicity, speed, sensitivity, affordability, and reliability* are five crucial ingredients to advance ammonia sensing and making it more accessible for both laboratory and field use. Although it is not a simple task to compare radically different detection concepts in terms of a single set of consistent metrics, we would like to briefly touch on a few associated aspects. Existing spectroscopic methods do not allow tracking of small changes in the concentration of ammonia and intermediate species on-site, not to mention *in situ* or *operando* observation in situations where the reaction mechanisms are not known. Most spectroscopic techniques and sensor approaches are directly or indirectly vulnerable to external laboratory or field environment, jeopardizing *reliability*. Although NMR and colorimetric methods excel in detection limits for overall concentration, it is important to remember that both approaches rely on the need for relatively large sensing volumes. For instance, strong signals are observed for a 1 mL volume at <1 ppm (parts per million) concentrations, which contains 10^{15}–10^{17} molecules of ammonia. For fundamental research, this means even greater number of molecules has to be produced at reactor heart to fulfill volume and sensitivity requirements for further analysis. This obstacle is elegantly overcome using surface-sensitive IR absorption spectroscopy, which is based on the principle of total attenuated reflection (ATR-FTIR) (Yao et al., 2018, 2020). This approach uniquely probes molecules produced right on the surface of electrode. It is a relatively fast and non-perturbative technique, requiring only tens of seconds for spectral acquisition. At the same time, the fixed experimental geometry, the necessity to isolate the IR light from the laboratory environment and the need for additional chemicals limit a broader implementation of the method.

In this work, we present a novel approach to ammonia detection, enabled through the use of surface-enhanced Raman scattering (SERS). This is a simple, fast, yet sensitive method that provides chemical selectivity to ammonia and does not rely on complex sensor design, specific beam path geometry, or chemical modifications of the solution. The method allows detection of sub-1 ppm ammonia concentrations in just under 1 s, which paves the way to ultrasensitive *operando* electrochemical experiments. Taking into account the short spatial reach of plasmonic enhancement, the observed signals correspond to as little as 10^4–10^5 molecules detected *locally* at the region of interest. SERS detection concept does not put any limitations on the identity or morphology of the electrode as long as it can be put close enough to SERS structure. The following can be easily engineered per specific experimental requirements to probe ammonia close to the electrode both on micro- and macro-scales—provide local reading of ammonia presence in closest proximity to the reaction site.

RESULTS

Figure 1A shows a representative spontaneous Raman spectrum of a concentrated ammonia solution spanning the molecular fingerprint region and the stretching modes of N-H, O-H, and C-H-related complexes. To understand the signatures of this spectrum, we performed a normal mode frequency analysis for ammonia and its aqueous formations via density functional theory (DFT) calculations, visualized in Figure 1B. These formations are addressed thoroughly in previous works and are most widely accepted contributors to vibrational spectrum of ammonia aqueous solution (Buckley and Ryder, 2017; Gardiner et al., 1973; Simonelli and Shultz, 2001; Sosa et al., 1996; Ujike and Tominaga, 2002; Yeo and Ford, 1991; Aggarwal et al., 2016; Langseth, 1932; Li and Keppler, 2014; Mysen and Fogel, 2010)—ammonia (NH_3), ammonium ion (NH_4^+), ammonia dimer (NH_3-NH_3), ammonia-water complex (NH_3-H_2O), and solvated ammonia complex (not shown in Figure 1).

Positions and relative intensities of the observed lines and their corresponding theoretical predictions are in excellent agreement. For more details on the DFT calculations and a table of the mode frequencies, see

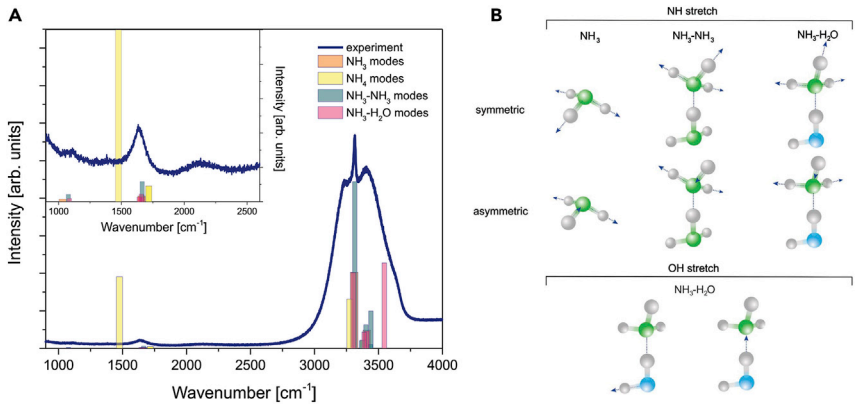

Figure 1. Raman Spectrum of Ammonia in Water and Calculated Spectral Positions Based on Various Stretching Modes

(A) Spontaneous Raman spectrum of bulk ammonia solution (0.3 wt%, 30,000 ppm). Exposure time 1 s. Column bars indicate positions of theoretically predicted bending, stretching, and rocking modes of ammonia-related formations.
(B) Main ammonia-related vibrations presented in stretching modes spectral region.

Methods and Supplementary Information. Although not very bright, several lines from monomer and dimer complexes are clearly visible in the fingerprint spectral region (Figure 1A, inset). Theory shows that, in contrast to the ammonia molecule, the ammonium ion should have the strongest presence in this frequency range through a 1,476 cm^{-1} contribution of an N-H deformation mode. Yet, the experimental absence of this line is confirmed through the evaluation of the NH_3/NH_4^+ mole ratio by pH measurements (see Methods). It should be noted that even 100 ppb ammonia dissolved in neutral pH solution consists of 95% ammonia molecules compared with ammonium ions. This agrees well with spectroscopy data, where only a broad line comprising H-N-H bending of NH_3, NH_3-NH_3, and NH_3-H_2O complexes is observed.

In contrast to the weak vibrational features in the fingerprint range, the stretching modes reveal clear signatures of ammonia's presence with intensities that are two orders of magnitude higher than fingerprint modes, in full agreement with DFT predictions. Although these ammonia-related peaks sit atop a strong background of water OH-stretching vibrations, we will show in this work that these signatures enable ammonia detection even at low concentration of the target. We expect the ammonia-related signals to remain clearly distinguishable even in other, more complex electrochemically relevant solutions. The CH-stretching mode of organic reagents (Figure S4) or different modes associated with dissolved salts are generally absent from the spectral region of interest.

The origin of the peaks in this spectral region and their positions has been thoroughly studied (Li and Keppler, 2014; Simonelli and Shultz, 2001; Srivastava et al., 1994; Ujike and Tominaga, 2002; Yeo and Ford, 1991) with the main peaks outlined in Table 1. From the perspective of relative intensities, the highest Raman signal corresponds to the N-H symmetric stretching mode that clearly stands out against the broad and complex O-H stretching band of water. According to DFT calculations, the asymmetric N-H stretching has 4 to 5 times smaller Raman intensity but strongly contributes to the broad profile of the overlapping water signals. Ujike et al. obtained the normal mode frequencies of the ammonia molecule, ammonia-ammonia dimer, and ammonia-water dimer by means of the GF matrix method (Ujike and Tominaga, 2002). In this method, the constants of the force matrix were determined from a direct fitting of the experimental data. In contrast, our approach utilizes force derivate matrices determined from first principles and as such relies on basic physical parameters of the compounds involved. For the ammonia monomer molecule, we obtained excellent agreement between this approach and previous works (Ujike and Tominaga, 2002; Zhao and Truhlar, 2008). However, for the complex dimer formations there are significant discrepancies. Although the lowest energies for ammonia and ammonia-water dimers have been determined at 3,217.4 and 3,044.1 cm^{-1}, respectively (Ujike and Tominaga, 2002), first principles anharmonic frequency calculations for dimer modes of NH_3-NH_3 and NH_3-H_2O do not differ by more than 10 cm^{-1}.

Moreover, our theoretical study did not find any ammonia normal modes at the lower energy side from the main peak at 3,260 cm^{-1}. The broad profile on which the main peak rests can be assigned to a distribution

Formation	Spectral Position	Intensity	Assignment
NH_3	3,409.0 cm^{-1}	36.8	NH asymmetric stretching
	3,309.8 cm^{-1}	155.8	NH symmetric stretching
NH_4+	3,380.0 cm^{-1}	16.8	NH asymmetric stretching
	3,276.8 cm^{-1}	101.0	NH symmetric stretching
NH_3-NH_3	3,441.0 cm^{-1}	76.2	NH asymmetric stretching
	3,438.0 cm^{-1}	7.8	NH asymmetric stretching
	3,402.3 cm^{-1}	48.2	NH asymmetric stretching
	3,369.5 cm^{-1}	15.6	NH asymmetric stretching
	3,315.4 cm^{-1}	341.6	NH symmetric stretching
NH_3-H_2O	3,545.6 cm^{-1}	175.0	OH stretching (H-bonded)
	3,410.9 cm^{-1}	35.3	NH asymmetric stretching
	3,389.2 cm^{-1}	33.0	NH asymmetric stretching
	3,305.0 cm^{-1}	155.31	NH symmetric stretching

Table 1. Main Ammonia-Related Vibrations Presented in Stretching Modes Spectral Region
For full mode list, please, see Table S1.

of additional contributions from solvated ammonia species, i.e., molecules that are engaged through multiple hydrogen bonds. At the high-energy side of the band, our predictions match previous estimates for ammonia-water complexes with non-bonded and bonded O-H stretches at 3,989 and 3,721 cm^{-1} (Yeo and Ford, 1991) (not shown in Figure 1B, see Table S1).

The strong peaks from the symmetric N-H stretch at ~3,300 cm^{-1} provide an opportunity to employ these spectroscopic signatures for tracing ammonia molecules or related reaction precursors. However, owing to the presence of the substantial water background and the weak response in the fingerprint range, Raman spectroscopy has long been considered unsuitable for ammonia detection. Indeed, regular Raman scattering is blind to solutions with concentrations below 1,000 ppm (Figure S1). To heighten and discriminate molecular signatures from the strong aqueous signals we employed surface-enhanced Raman scattering (SERS), a well-known approach to detect analytes down to single molecule limit (Blackie et al., 2009; Yampolsky et al., 2014). The broadly accepted electromagnetic theory for enhancement relies on excitation of localized surface plasmons (LSP), which provide strongly localized fields that can enhance the optical response of molecules in their vicinity. Surprisingly, SERS has not been specifically utilized for ammonia detection, although some basic principles of the effect in relation to ammonia has been demonstrated in 1984 in work by Sanchez et al. (1984) Further studies on detection of ammonium nitride revealed sensitive detection limits in fingerprint branch (Farrell et al., 2014), even though all the observed and discussed lines are not related to NH_3, but rather NO_3^-. Recently the possibility of ammonia detection with excitation on the slope of plasmonic resonance has been discussed (Nazemi et al., 2020; Nazemi, 2020). In this work, an elegant implementation of SERS detection for live reaction monitoring was discussed with acquisition time constants of ~10 s. Although the authors focused mainly on the fingerprint region and sidebands from probable ammonia-water dimers, no stretching peak of the NH_3 monomer has been observed in *operando* experiments.

Ammonia Detection with Commercial SERS Substrates

For our first initial demonstration of ultrasensitive ammonia detection via SERS we used a conventional confocal microscopy setup and commercially available SERS substrates (SERStrate, Silmeco, Denmark). The substrates consist of leaning silicon nanopillars covered with silver (Schmidt et al., 2012). The structure forms a rather dense and homogeneous distribution of metal covered clusters of 50–100 nm with corresponding plasmonic resonances that closely match the excitation wavelength of 532 nm. The aqueous ammonia solution was confined between the SERS substrate and the microscope slide, with the Raman

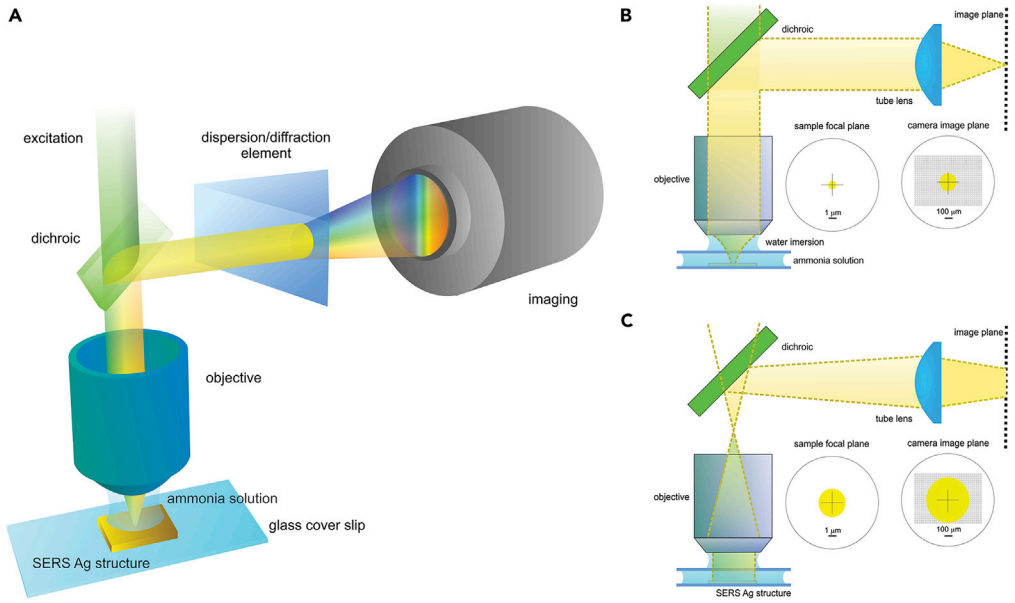

Figure 2. Concept of Experimental Approach

(A–C) (A) Epi detection of Raman signal, (B) confocal detection for high spatial resolution, (C) wide-field detection approach for large volume probing.

signal collected in the epi-geometry by a water immersion objective and coupled into a CCD-based spectrometer (Figure 2A, see Methods for details). The setup was used in two regimes—confocal and wide-field approach (Figures 2B and 2C). The confocal collection geometry allows probing of fine local ammonia concentrations at the region of interest. For the given experimental conditions and the numerical aperture of the collection objective, this volume corresponds to only ~1.2 μm^3 or 1.2 fL of solution being probed. To enable excitation within a wider region of interest, the beam was focused at the back aperture of the excitation/collection objective and the imaging aperture/slit was effectively removed from the image plane. The latter allowed for an increased focal volume by almost an order of magnitude, as well as a more effective use of the detector area without significantly losing spectral resolution (4 cm^{-1}). Hence, this wide-field imaging mode greatly improves detection sensitivity (Figure S2).

A typical SERS spectrum of an aqueous ammonia solution is shown in Figure 3, acquired using confocal geometry and at only 200 ppm concentration (Figure 2B). Strong ammonia SERS signals clearly overcome the water background compared with the spontaneous Raman signal of the bulk solution. The bright line around ~3,260 cm^{-1} indicates high sensitivity to the symmetric N-H stretching mode with an improvement of the detection limit by a 1000-fold relative to regular Raman spectroscopy. The spectral shift (~50 cm^{-1}) and line broadening are anticipated owing to the molecule-surface interaction, with the main line of the NH_3 monomer linewidth changed from 14 (for spontaneous Raman) to 30 cm^{-1} (for SERS). Overall, the spectral shape corroborates theoretical predictions and can be closely reproduced with a simple Gaussian broadening of the NH_3 monomer and NH_3-H_2O dimer modes (see Table S2). Note the rather strong presence of additional spectral structures around 2,930 cm^{-1} that were not visible in spontaneous Raman measurements of bulk solution (Figure S2A) but are found at certain locations on the substrate through SERS (Figure S3). Further experiments confirmed that these signals do not scale similarly with ammonia concentration and N-H-related bands. These lines were also occasionally observed in SERS of pure Millipore water. Additional experiments and simple line shape analysis suggest that these signals can be assigned to the strong C-H stretching modes of occasional organic contamination on the plasmonic structure (Figure S4). These characteristic modes in the C-H stretching spectral range are well known and can be confidently used for identifying organic species in bio-related environments (Faiman and Larsson, 1976; Yu et al., 2013).

The SERS signal dependence on the ammonia concentration gives rather important insights into the actual chemical content of the solution. As observed in Figure 4A, for higher-concentration solutions the

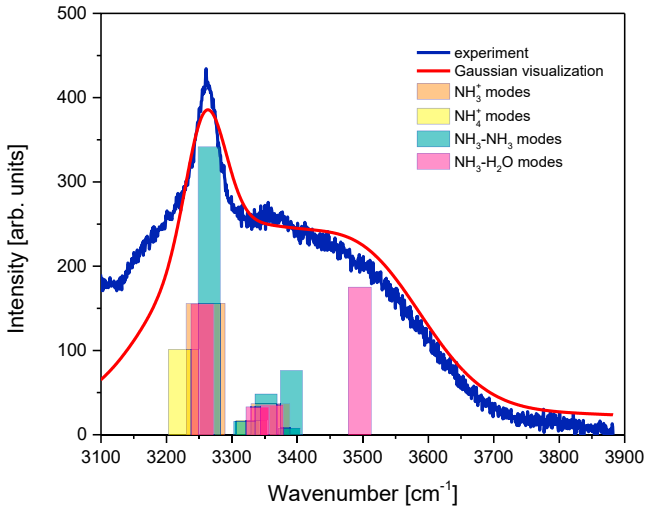

Figure 3. Calculated Modes for Ammonia-Related Structure Overlaid with SERS Spectrum of 200 ppm Ammonia Solution

Red curve is visualization through using Gaussian line shapes at predicted theoretical positions for NH_3 and NH_3-H_2O only. Exposure time 0.3 s.

ammonia-related bands dominate the bulk water background with broad and rich spectral features in the stretching mode region. With a decrease of concentration, the spectrum evolves into a steady plateau—the broad O-H spectrum of bulk water molecules. A detailed analysis of the integrated intensity for the bright spectral feature around 3,260 cm^{-1} reveals clear linear behavior as a function of ammonia concentration (Figure 4B). The following means that signals in this range are dependent on complexes that contain a single NH_3 molecule, i.e., the NH_3 monomer and the NH_3-H_2O dimer, as any signal response from NH_3-NH_3 dimers is anticipated to be quadratic. We stress that all observations are fully reversible when concentration levels are changed on the same SERS substrate, as shown in Figure S5. This points to the absence of a strong chemical interaction with the metal surface and thus allows reversible use of the sensor over a large dynamic range of the ammonia concentration.

Figures 4 and 5 illustrate the detection sensitivity of the approach. We note that all spectra have been acquired without any signal processing, modulation or electronic filtering. Acquisition times did not exceed 2 s to reveal the true and unperturbed potential of the method.

For the given plasmonic structure, collection efficiencies, and experimental geometries, 1-ppm concentrations of ammonia can be clearly observed for measurement times of 1 s or less. For longer acquisition times of 1–2 s the detection limit of few hundreds of ppb is easily attainable (Figure S6).

In this work, we report the method's sensitivity in terms of molecular concentration of ammonia in bulk solution. At the same time, owing to specifics of SERS-based method, i.e., sensitivity to local molecular presence, it is helpful to express sensitivity in terms of an alternative metric, namely, the estimated number of molecules probed. This metric relies on the assumption that (1) the plasmonic enhancement is short ranged (Bouhelier and Novotny, 2007) and (2) ammonia signals from bulk solutions are negligible at these concentrations (Figure S1). For the confocal geometry experiments with a 1.2-fL probe volume, a 1-ppm concentration corresponds to only 10^4–10^5 molecules—the amount necessary for spectroscopic observation (Table S3). The local sensitivity limit, and thus the molecular detection limit, is already significantly smaller compared with competing methods; these numbers are still conservative estimates. The estimation relies on the total amount of molecules in the confocal volume with Rayleigh range of about ~1.5 μm. In reality, only those molecules that are in near-field proximity (<1 nm) to the metal structure are contributing to the signal. Thus, the actual number of sampled molecules may still be a few orders of magnitude smaller. In the wide-field illumination approach, the surface area efficiently increases just under ten times, thus probing a greater number of molecules contained within the detection area.

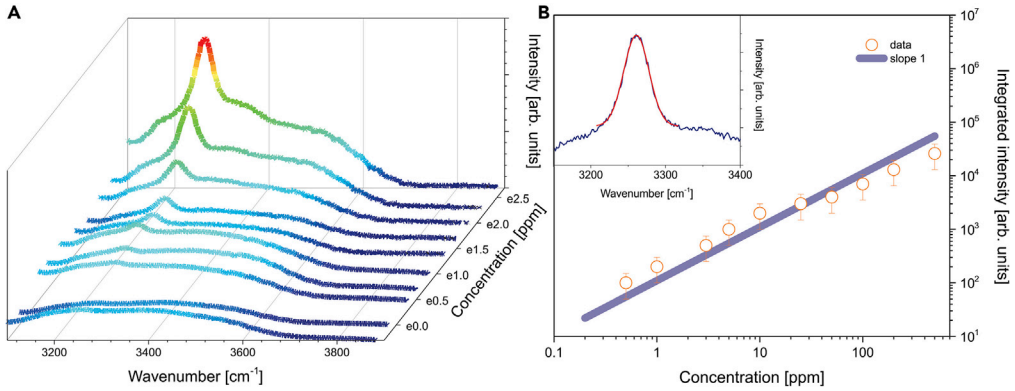

Figure 4. Concentration Dependence Studies

(A) Spectral evolution as a function of ammonia concentration.

(B) Integrated intensity of 3,260 cm^{-1} spectral line. Blue straight line represents linear function with slope 1. Inset: Gaussian fit of ammonia-related line for 200 ppm solution. Exposure time 1 s. Integrated signal intensity is determined with under 10% error for the smallest concentrations and the signal fluctuations are considered negligible compared with spatial reproducibility within the same substrate, that varies on average by the factor of 2 (error over 10 experiments for each given concentration).

Ammonia Detection on Ag Ink

We have performed further experiments based on a similar detection concept, but that employs less sophisticated plasmonic structures to explore more affordable sensor alternatives. For this purpose, we used a commercially available Ag ink (Sigma Aldrich), based on metal nanoparticles. This material is widely used for printable conductors, antibacterial material filters, thin film electronics, etc. This particular ink is based on silver particles (d_{90} = 115 nm, d_{50} = 70 nm) with plasmonic resonances that match our previous experiments. When drop casted and dried on mica glass slide, the colloidal suspension forms a homogeneous mirror-like film. Optical microscopy and SEM images of the film are shown in Figures 6A and 6B, respectively. Despite its simplicity, the ink-based SERS substrate permits clear observations of signals with a sub-1 ppm detection limit for ammonia (Figure 6C). Although the enhancement, spatial distribution, and reproducibility are on par with commercial SERS substrates, the approach can be improved by adopting better controlled and cleaner printing procedures.

DISCUSSION

The SERS method discussed in this work offers a new approach for detecting ammonia and related complexes with a chemical sensitivity that is competitive with that of other spectroscopic techniques, while at the same time being straightforward and affordable in its implementation.

For the *low limit of detection*, the method is on par with other spectroscopic techniques that allow detection of concentration under 1 ppm. Note that the physical principle of plasmonic enhancement does not put any fundamental limitations on the phase of the sample, allowing trace detection in both liquid and gaseous phases. Using basic assumptions for the spatial extent of the local fields and the size of the illumination spot, 1 ppm overall solution concentration corresponds to 10^4–10^5 molecules in probed volume. However, such sensitivity does not come at the expense of long acquisition time. The acquisition *speed* easily allows live observations—sub-second detection of only 1 ppm concentration or a few thousands of molecules locally at the region of interest makes *in situ* monitoring of chemical reaction possible.

As an optical-based approach, it allows distant, nonperturbative (non-consuming) probing, thus offering clean and *reliable* experiments. Moreover, molecules do not appear to strongly bind to the surface, making observations *reversible* as the molecular content is changed.

The practical implementation of the concept introduced in this work can be significantly improved, in particular in terms of speed and sensitivity. The SERS signal enhancement factors rely on the interplay between spectral position of the plasmonic resonance, excitation source wavelength, and the intrinsic spectral response of the molecule. Thus, fine-tuning of the metal particle size and the structure arrangement

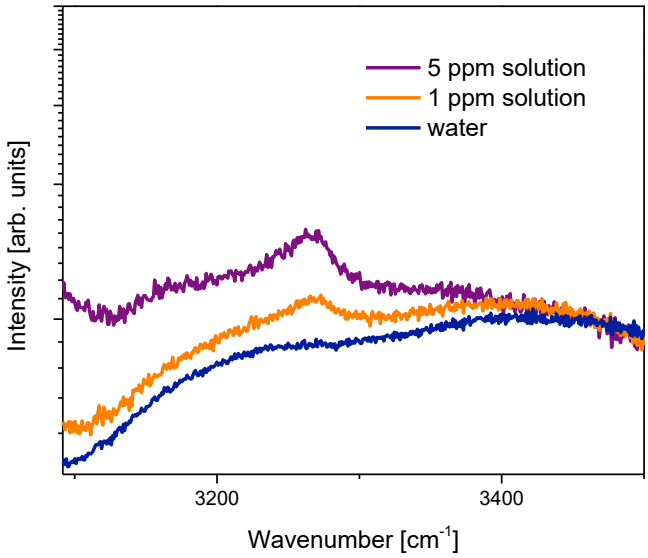

Figure 5. Fast Detection of Low Amount of Ammonia Using Commercial Ag-Coated Si Nanopillars Substrate
Exposure time 1 s.

may result in a significant improvement of detection limits. Although commercially available SERS substrates are excellent initial choice, they require complex production and are currently too expensive for up-scaling. We demonstrate that simple deposition of colloidal silver ink on the substrate of choice already gives comparable results. Hence, the method does not require special facilities and procedures to produce *affordable* SERS sensors.

Lastly, the *simplicity* of the method is of key significance to broad implementation. With flexible beam positioning, measurements can be performed at any region of interest within a given environment or chemical cell. Through point scanning or a wide-field imaging mode, the method allows sampling of the spatial distribution of ammonia content. This flexibility has the potential to provide important insights in underlying reactions mechanisms, which is especially relevant for solid-liquid interfaces. In addition, in our experiments with confocal signal collection we have used no more than 1.5 mW CW laser light, light doses that are easily attained with compact and inexpensive laser diode modules. Furthermore, the method can be adapted for use with lower numerical aperture lenses, whereby the lower collection efficiency is offset by a larger illumination area. By probing a greater number of molecules in larger spot sizes, long focusing approach may prove to be advantageous for sensing needs that do not require spatial confinement and resolution.

As underlined in this work, the Raman spectrum in the N-H stretching region is rich in NH_3-related signals. Detection of this broadband spectral region, as opposed to the narrow NH_3 monomer line alone, will result in drastic improvements of detection limits. The large Stokes shift of this spectral window makes it possible to use simple colored glass Schott filters, rather than expensive sharp-edge Raman dichroic mirrors. Finally, conventional single-pixel Si detectors can be used. Although cheap and affordable, such detectors can match standard charged-coupled devices, when using photo-multipliers and avalanche mode detectors can even boost the sensitivity. All these potential simplifications will allow the design of a simple and robust device to be used for field research or in-line production.

Ammonia detection method through SERS converges *simplicity* and *affordability* with *speed* and *sensitivity*. It has potential to be greatly popularized and help to overcome several roadblocks that have been slowing fundamental and applied chemical research in these areas for many decades.

Limitations of the Study

Thin Ag film is expected to easily oxidize. Although no oxidation has been observed within the time frame of the experiments (several hours) for ink-based substrates, strong coloration, hence oxidation, of film

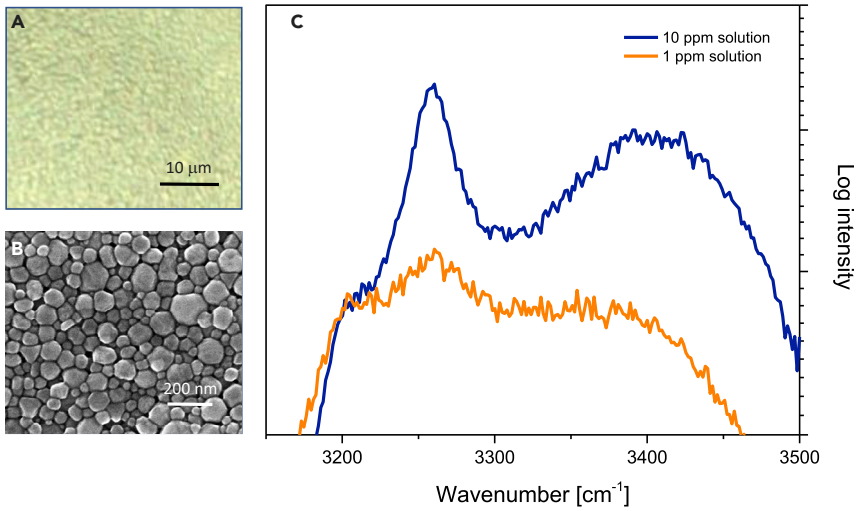

Figure 6. Fast Detection of Low Amount of Ammonia Using Drop Casted Ag Ink on a Glass Slide
(A–C) (A) Optical image of dried Ag ink, (B) SEM image of dried Ag ink, (C) SERS signal on custom made SERS substrate. Exposure time 1 s.

becomes visible if left for several days in open laboratory environment. The following put the restrictions on substrate handling if considered for long-term use.

Resource Availability

Lead Contact

Further information and requests for resources and reagents should be directed to and will be fulfilled by the Lead Contact, Dmitry Fishman (dmitryf@uci.edu).

Materials Availability

This study did not generate new unique reagents.

Data and Code Availability Statements

No code has been used to analyze or process the data. Original data are available from the corresponding author on request.

METHODS

All methods can be found in the accompanying Transparent Methods supplemental file.

SUPPLEMENTAL INFORMATION

Supplemental Information can be found online at https://doi.org/10.1016/j.isci.2020.101757.

ACKNOWLEDGMENTS

This work was supported in part by a subcontract from DOE-EERE Advanced Manufacturing Office award to Sandia National Laboratories (AOP 34920). D.A.F. would like to thank Prof. Vartkess A. Apkarian for inspiring discussions. D.A.F. acknowledges NSF grant CHE-0960179. I.M. wishes to thank the UNM Center for Advanced Research Computing for computational resources. Authors are thankful to Dr. Andrea Perego, National Fuel Cell Research Center (NFCRC), University of California Irvine for the SEM images obtained at Irvine Materials Research Institute (IMRI).

AUTHOR CONTRIBUTIONS

D.A.F. and P.A. conceived the idea and supervised the study. Y.L. prepared ammonia solutions. Y.L., T.A., and Y.C. directed general logistics of chemical experiments. I.M. performed DFT calculations. D.A.F.

designed experimental concepts, conducted optical experiments, analyzed the data, and wrote initial manuscript. All authors took part in thorough discussions of data and contributed to its understanding. All authors contributed to manuscript editing.

DECLARATION OF INTERESTS

All authors declare no competing interests.

Received: September 17, 2020
Revised: October 20, 2020
Accepted: October 28, 2020
Published: November 20, 2020

REFERENCES

Aggarwal, R.L., Farrar, L.W., Cecca, S.D., and Jeys, T.H. (2016). Raman spectra and cross sections of ammonia, chlorine, hydrogen sulfide, phosgene, and sulfur dioxide toxic gases in the fingerprint region 400-1400 cm−1. AIP Adv. *6*, 025310.

Ahmadi Tabr, F., Salehiravesh, F., Adelnia, H., Gavgani, J.N., and Mahyari, M. (2019). High sensitivity ammonia detection using metal nanoparticles decorated on graphene macroporous frameworks/polyaniline hybrid. Talanta *197*, 457–464.

Ampuero, S., and Bosset, J.O. (2003). The electronic nose applied to dairy products: a review. Sensor. Actuat. B Chem. *94*, 1–12.

Andersen, S.Z., Čolić, V., Yang, S., Schwalbe, J.A., Nielander, A.C., McEnaney, J.M., Enemark-Rasmussen, K., Baker, J.G., Singh, A.R., Rohr, B.A., et al. (2019). A rigorous electrochemical ammonia synthesis protocol with quantitative isotope measurements. Nature *570*, 504–508.

Baird, R., and Bridgewater, L. (1995). Standard Methods for the Examination of Water and Wastewater (American Public Health Association).

Blackie, E.J., Le Ru, E.C., and Etchegoin, P.G. (2009). Single-molecule surface-enhanced Raman spectroscopy of nonresonant molecules. J. Am. Chem. Soc. *131*, 14466–14472.

Bolleter, W.T., Bushman, C.J., and Tidwell, P.W. (1961). Spectrophotometric determination of ammonia as indophenol. Anal. Chem. *33*, 592–594.

Bosch, C. (1908). Process of Producing Ammonia (U.S. Patent No. 990).

Bouhelier, A., and Novotny, L. (2007). Near-field Optical Excitation and Detection of Surface Plasmons', *Surface Plasmon Nanophotonics* (Springer), pp. 139–153.

Buckley, K., and Ryder, A.G. (2017). Applications of Raman spectroscopy in biopharmaceutical manufacturing: a short review. Appl. Spectrosc. *71*, 1085–1116.

Cai, Q.Y., Jain, M.K., and Grimes, C.A. (2001). A wireless, remote query ammonia sensor. Sensor. Actuat. B Chem. *77*, 614–619.

Chabukswar, V.V., Pethkar, S., and Athawale, A.A. (2001). Acrylic acid doped polyaniline as an ammonia sensor. Sensor. Actuat. B Chem. *77*, 657–663.

Chang, S.C., Stetter, J.R., and Cha, C.S. (1993). Amperometric gas sensors. Talanta *40*, 461–477.

Chen, J.G., Crooks, R.M., Seefeldt, L.C., Bren, K.L., Bullock, R.M., Darensbourg, M.Y., Holland, P.L., Hoffman, B., Janik, M.J., Jones, A.K., et al. (2018). Beyond fossil fuel–driven nitrogen transformations. Science *360*, eaar6611.

Clifford, P.K., and Tuma, D.T. (1982). Characteristics of semiconductor gas sensors I. Steady state gas response. Sensors Actuators *3*, 233–254.

Cui, X., Tang, C., and Zhang, Q. (2018). A review of electrocatalytic reduction of dinitrogen to ammonia under ambient conditions. Adv. Energy Mater. *8*, 1800369.

Docquier, N., and Candel, S. (2002). Combustion control and sensors: a review. Prog. Energy Combust. Sci. *28*, 107–150.

Faiman, R., and Larsson, K. (1976). Assignment of the C—H stretching vibrational frequencies in the Raman spectra of lipids. J. Raman Spectrosc. *4*, 387–394.

Farrell, M.E., Holthoff, E.L., and Pellegrino, P.M. (2014). Surface-enhanced Raman scattering detection of ammonium nitrate samples fabricated using drop-on-demand inkjet technology. Appl. Spectrosc. *68*, 287–296.

Gardiner, D., Hester, R., and Grossman, W. (1973). Ammonia in the liquid state and in solution: a Raman study. J. Raman Spectrosc. *1*, 87–95.

Giovannozzi, A.M., Pennecchi, F., Muller, P., Balma Tivola, P., Roncari, S., and Rossi, A.M. (2015). An infrared spectroscopy method to detect ammonia in gastric juice. Anal. Bioanal. Chem. *407*, 8423–8431.

Guo, H., and Tao, S. (2007). Silver nanoparticles doped silica nanocomposites coated on an optical fiber for ammonia sensing. Sensor. Actuat. B Chem. *123*, 578–582.

Haber, F. (1905). Thermodynamik Technischer Gasreaktionen (Salzwasser Verlag).

Heiduschka, P., Preschel, M., Rösch, M., and Göpel, W. (1997). Regeneration of an electropolymerised polypyrrole layer for the amperometric detection of ammonia. Biosens. Bioelectron. *12*, 1227–1231.

Hübner, H.P., and Drost, S. (1991). Tin oxide gas sensors: an analytical comparison of gas-sensitive and non-gas-sensitive thin films. Sensor. Actuat. B Chem. *4*, 463–466.

Imawan, C., Solzbacher, F., Steffes, H., and Obermeier, E. (2000). Gas-sensing characteristics of modified-MoO3 thin films using Ti-overlayers for NH3 gas sensors. Sensor. Actuat. B Chem. *64*, 193–197.

Kohl, D. (2001). Function and applications of gas sensors. J. Phys. D Appl. Phys. *34*, R125–R149.

Kukla, A.L., Shirshov, Y.M., and Piletsky, S.A. (1996). Ammonia sensors based on sensitive polyaniline films. Sensor. Actuat. B Chem. *37*, 135–140.

Lähdesmäki, I., Kubiak, W.W., Lewenstam, A., and Ivaska, A. (2000). Interferences in a polypyrrole-based amperometric ammonia sensor. Talanta *52*, 269–275.

Lähdesmäki, I., Lewenstam, A., and Ivaska, A. (1996). A polypyrrole-based amperometric ammonia sensor. Talanta *43*, 125–134.

Langseth, A. (1932). Feinstruktur von Ramanbanden - II. Das ramanspektrum von Ammoniak in wässeriger lösung. Z. für Physik *77*, 60–71.

Li, Y., and Keppler, H. (2014). Nitrogen speciation in mantle and crustal fluids. Geochimica et Cosmochimica Acta *129*, 13–32.

Lundström, I., Svensson, C., Spetz, A., Sundgren, H., and Winquist, F. (1993). From hydrogen sensors to olfactory images - twenty years with catalytic field-effect devices. Sensor. Actuat. B. Chem. *13*, 16–23.

Lv, D., Chen, W., Shen, W., Peng, M., Zhang, X., Wang, R., Xu, L., Xu, W., Song, W., and Tan, R. (2019). Enhanced flexible room temperature ammonia sensor based on PEDOT: PSS thin film with FeCl3 additives prepared by inkjet printing. Sensor. Actuat. B Chem. *298*, 126890.

Mahendran, V., and Philip, J. (2013). An optical technique for fast and ultrasensitive detection of ammonia using magnetic nanofluids. Appl. Phys. Lett. *102*, 063107.

Max, J.-J., and Chapados, C. (2013). Aqueous ammonia and ammonium chloride hydrates: principal infrared spectra. J. Mol. Struct. *1046*, 124–135.

Mount, G.H., Rumburg, B., Havig, J., Lamb, B., Westberg, H., Yonge, D., Johnson, K., and Kincaid, R. (2002). Measurement of atmospheric ammonia at a dairy using differential optical absorption spectroscopy in the mid-ultraviolet. Atmos. Environ. *36*, 1799–1810.

Mysen, B.O., and Fogel, M.L. (2010). Nitrogen and hydrogen isotope compositions and solubility in silicate melts in equilibrium with reduced (N+H)-bearing fluids at high pressure and temperature: effects of melt structure. Am. Mineral. *95*, 987–999.

Nazemi, M. (2020). Investigation of (Photo) Electrocatalytic Conversion of Dinitrogen to Ammonia Using Hybrid Plasmonic Nanostructures (Georgia Institute of Technology).

Nazemi, M., Soule, L., Liu, M., and El-Sayed, M.A. (2020). Ambient ammonia electrosynthesis from nitrogen and water by incorporating palladium in bimetallic gold–silver nanocages. J. Electrochem. Soc. *167*, 054511.

Nicolas-Debarnot, D., and Poncin-Epaillard, F. (2003). Polyaniline as a new sensitive layer for gas sensors. Anal. Chim. Acta *475*, 1–15.

Nielander, A.C., McEnaney, J.M., Schwalbe, J.A., Baker, J.G., Blair, S.J., Wang, L., Pelton, J.G., Andersen, S.Z., Enemark-Rasmussen, K., Čolić, V., et al. (2019). A versatile method for ammonia detection in a range of relevant electrolytes via direct nuclear magnetic resonance techniques. ACS Catal. *9*, 5797–5802.

Palmqvist, E., Berggren Kriz, C., Svanberg, K., Khayyami, M., and Kriz, D. (1995). DC-resistometric urea sensitive device utilizing a conducting polymer film for the gas-phase detection of ammonia. Biosens. Bioelectron. *10*, 283–287.

Patton, C.J., and Crouch, S.R. (1977). Spectrophotometric and kinetics investigation of the Berthelot reaction for the determination of ammonia. Anal. Chem. *49*, 464–469.

Qing, G., Ghazfar, R., Jackowski, S.T., Habibzadeh, F., Ashtiani, M.M., Chen, C.-P., Smith, M.R., and Hamann, T.W. (2020). Recent advances and challenges of electrocatalytic N2 reduction to ammonia. Chem. Rev. *120*, 5437–5516.

Riegel, J., Neumann, H., and Wiedenmann, H.M. (2002). Exhaust gas sensors for automotive emission control. Solid State Ion. *152-153*, 783–800.

Sanchez, L.A., Lombardi, J.R., and Birke, R.L. (1984). Surface enhanced Raman scattering of ammonia. Chem. Phys. Lett. *108*, 45–50.

Schmidt, M.S., Hübner, J., and Boisen, A. (2012). Large area fabrication of leaning silicon nanopillars for surface enhanced Raman spectroscopy. Adv. Mater. *24*, OP11–OP18.

Searle, P.L. (1984). The berthelot or indophenol reaction and its use in the analytical-chemistry of nitrogen - a review. Analyst *109*, 549–568.

Simonelli, D., and Shultz, M.J. (2001). Temperature dependence for the relative Raman cross section of the ammonia/water complex. J. Mol. Spectrosc. *205*, 221–226.

Sosa, C.P., Carpenter, J.E., and Novoa, J.J. (1996). Structures and interaction energies of mixed dimers of NH3 H2O, and HF by Hartree-Fock, møller-Plesset, and density-functional methodologies. In Chemical Applications of Density-Functional Theory, *629*, B.L. Brian, B.R. Richard, and Z. Tom, eds., pp. 131–141.

Srivastava, R.K., Lal, P., Dwivedi, R., and Srivastava, S.K. (1994). Sensing mechanism in tin oxide-based thick-film gas sensors. Sensor. Actuat. B Chem. *21*, 213–218.

Tang, C., and Qiao, S.Z. (2019). How to explore ambient electrocatalytic nitrogen reduction reliably and insightfully. Chem. Soc. Rev. *48*, 3166–3180.

Timmer, B., Olthuis, W., and Berg, A.v. d. (2005). Ammonia sensors and their applications—a review. Sensor. Actuat. B Chem. *107*, 666–677.

Tzollas, N.M., Zachariadis, G.A., Anthemidis, A.N., and Stratis, J.A. (2010). A new approach to indophenol blue method for determination of ammonium in geothermal waters with high mineral content. Int. J. Environ. Anal. Chem. *90*, 115–126.

Ujike, T., and Tominaga, Y. (2002). Raman spectral analysis of liquid ammonia and aqueous solution of ammonia. J. Raman Spectrosc. *33*, 485–493.

Wang, X., Miura, N., and Yamazoe, N. (2000). Study of WO3-based sensing materials for NH3 and NO detection. Sensor. Actuat. B Chem. *66*, 74–76.

Xu, C., Miura, N., Ishida, Y., Matsuda, K., and Yamazoe, N. (2000). Selective detection of NH3 over NO in combustion exhausts by using Au and MoO3 doubly promoted WO3 element. Sensor. Actuat. B Chem. *65*, 163–165.

Yamazoe, N. (1991). New approaches for improving semiconductor gas sensors. Sensor. Actuat. B Chem. *5*, 7–19.

Yampolsky, S., Fishman, D.A., Dey, S., Hulkko, E., Banik, M., Potma, E.O., and Apkarian, V.A. (2014). Seeing a single molecule vibrate through time-resolved coherent anti-Stokes Raman scattering. Nat. Photon. *8*, 650–656.

Yao, Y., Zhu, S., Wang, H., Li, H., and Shao, M. (2020). A spectroscopic study of electrochemical nitrogen and nitrate reduction on rhodium surfaces. Angew. Chem. Int. Ed. Engl. *59*, 10479–10483.

Yao, Y., Zhu, S., Wang, H., Li, H., and Shao, M. (2018). A spectroscopic study on the nitrogen electrochemical reduction reaction on gold and platinum surfaces. J. Am. Chem. Soc. *140*, 1496–1501.

Yeo, G.A., and Ford, T.A. (1991). The matrix isolation infrared spectrum of the water—ammonia complex. Spectrochim. Acta A Mol. Spectrosc. *47*, 485–492.

Yu, Y., Wang, Y., Lin, K., Hu, N., Zhou, X., and Liu, S. (2013). Complete Raman spectral assignment of methanol in the C–H stretching region. J. Phys. Chem. A *117*, 4377–4384.

Zakrzewska, K. (2001). Mixed oxides as gas sensors. Thin Solid Films *391*, 229–238.

Zhao, Y., Shi, R., Bian, X., Zhou, C., Zhao, Y., Zhang, S., Wu, F., Waterhouse, G.I.N., Wu, L.-Z., Tung, C.-H., and Zhang, T. (2019). Ammonia detection methods in photocatalytic and electrocatalytic experiments: how to improve the reliability of NH3 production rates? Adv. Sci. *6*, 1802109.

Zhao, Y., and Truhlar, D.G. (2008). The M06 suite of density functionals for main group thermochemistry, thermochemical kinetics, noncovalent interactions, excited states, and transition elements: two new functionals and systematic testing of four M06-class functionals and 12 other functionals. Theor. Chem. Acc. *120*, 215–241.

Zilberman, Y., Chen, Y., and Sonkusale, S.R. (2014). Dissolved ammonia sensing in complex mixtures using metalloporphyrin-based optoelectronic sensor and spectroscopic detection. Sensor. Actuat.B Chem. *202*, 976–983.

iScience, Volume *23*

Supplemental Information

Facile All-Optical Method for *In Situ* Detection of Low Amounts of Ammonia

Yuanchao Liu, Tristan Asset, Yechuan Chen, Eamonn Murphy, Eric O. Potma, Ivana Matanovic, Dmitry A. Fishman, and Plamen Atanassov

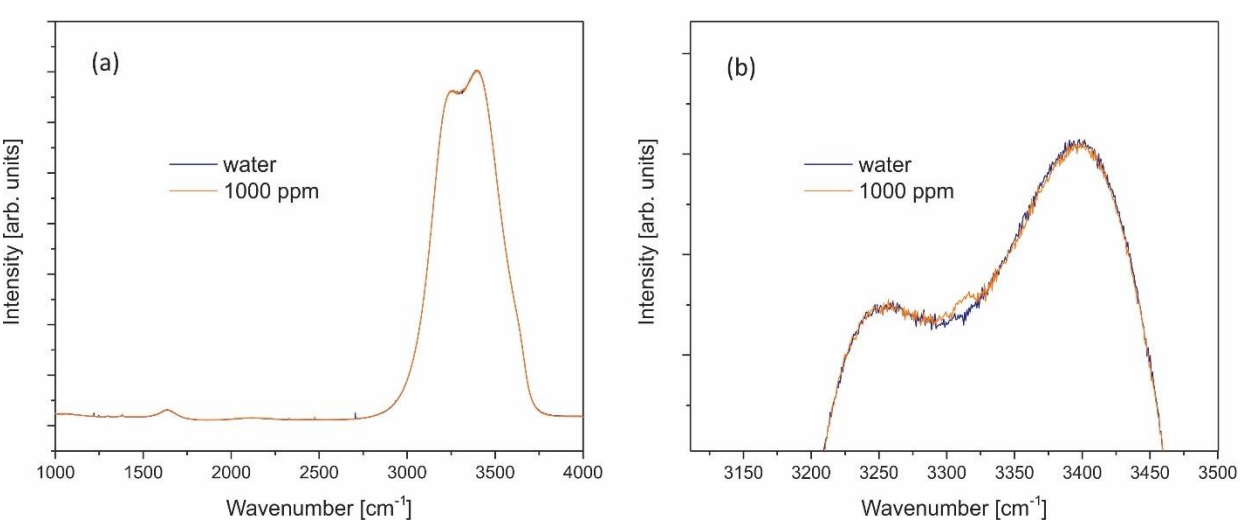

Figure SF1. (a) Spontaneous Raman spectra of water and 1000 ppm ammonia solution. (b) Zoomed part of spontaneous Raman spectra around NH_3 symmetric mode (~3300 cm^{-1}). Exposure time 1s. Related to Figure 1.

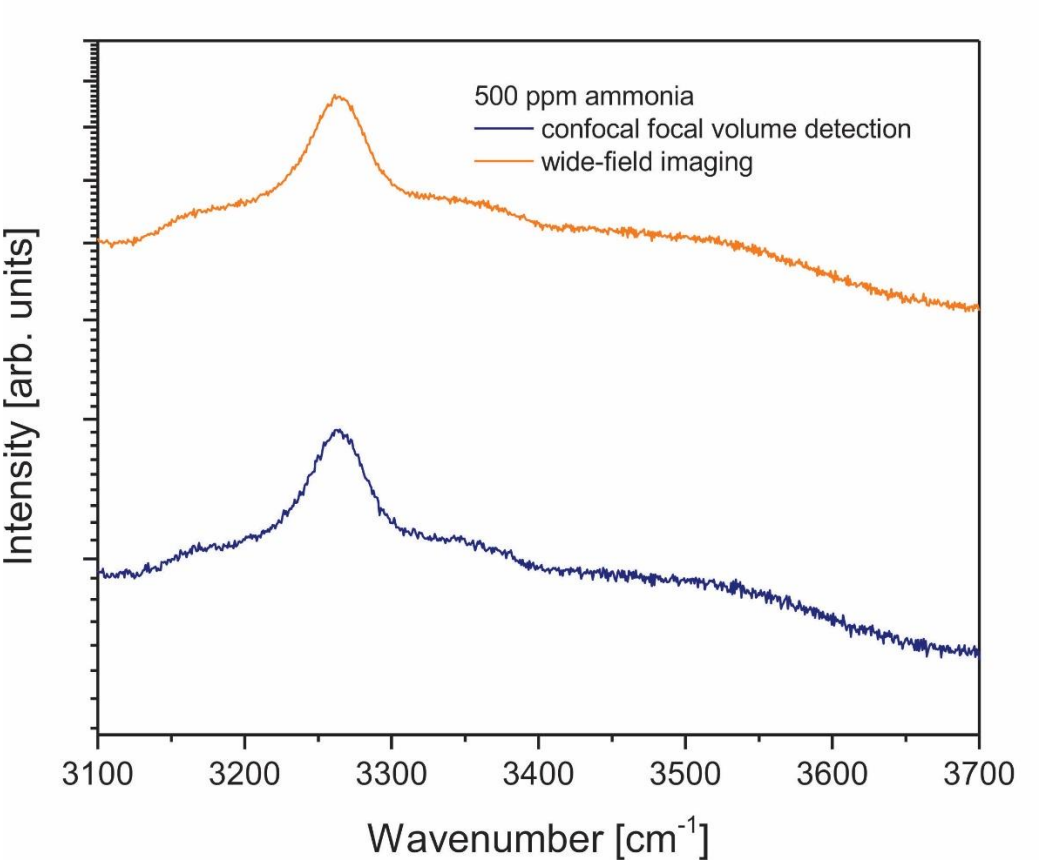

Figure SF2. Direct comparison of confocal imaging and wide-field detection approach. Exposure time 0.3 s. Related to Figure 2.

Table ST2. Parameters used for simple Gaussian visualization. No fitting has been done. Related to Figure 3.

Formation	Parameter	Value
NH_3	Spectral position	3409.0 cm^{-1}
	Amplitude	36.8
	Width	200 cm^{-1}
	Spectral position	3309.8 cm^{-1}
	Amplitude	155.8
	Width	30 cm^{-1}
NH_3-H_2O	Spectral position	3545.6 cm^{-1}
	Amplitude	175
	Width	200 cm^{-1}
	Spectral position	3410.9 cm^{-1}
	Amplitude	35.3
	Width	200 cm^{-1}
	Spectral position	3389.2 cm^{-1}
	Amplitude	33.0
	Width	200 cm^{-1}
	Spectral position	3305.0 cm^{-1}
	Amplitude	155.31
	Width	200 cm^{-1}

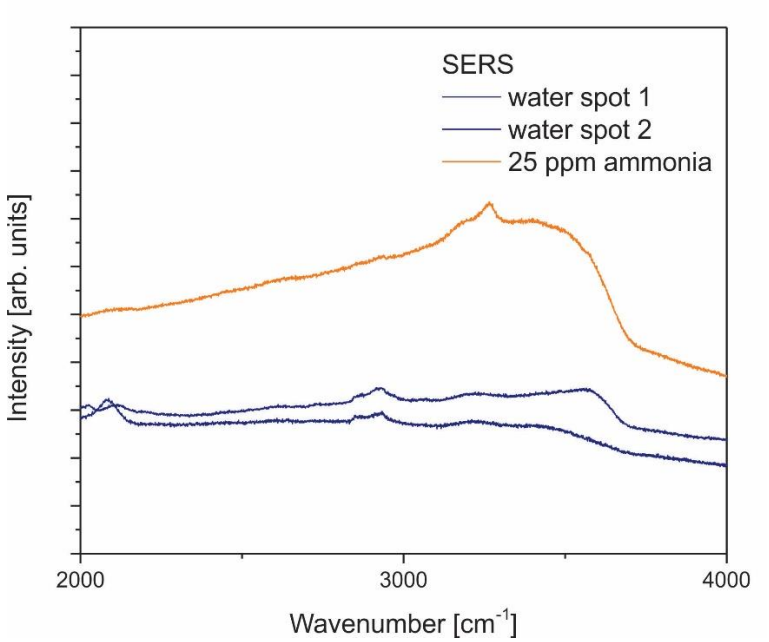

Figure SF3. SERS spectrum of 25 ppm ammonia solution and water in different spots on substrate. Line at ~2900 cm^{-1} has no concentration correlation similar to line at 3260 cm^{-1}. Exposure time 1s. related to Table 1 and Figure 3.

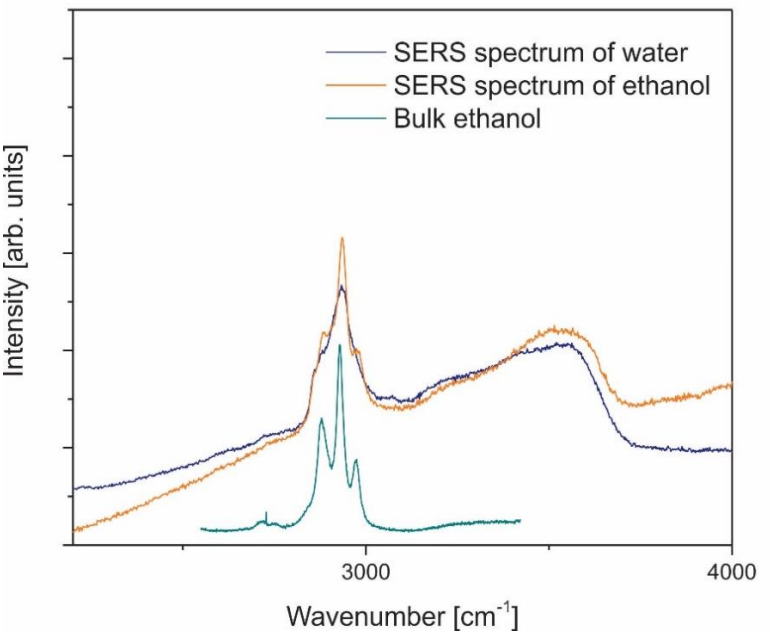

Figure SF4. Normalized SERS spectrum of water, ethanol overlaid with spontaneous Raman spectrum of ethanol. Line position and spectral structure indicates contamination of SERS substrate with organic compound sporadically distributed on substrate. SERS spectra clearly shows broadened lines with respect to spontaneous Raman signals, which is expected for molecule-metal interaction. Exposure time 1s. Related to Figure 3.

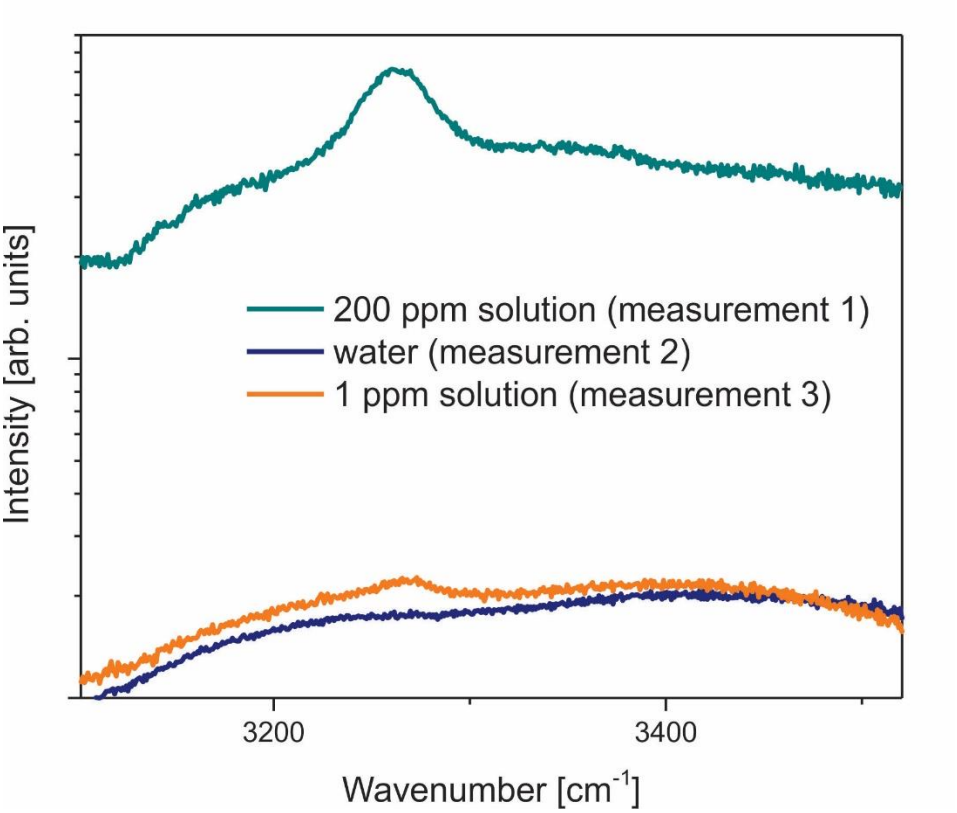

Figure SF5. SERS on Ag plasmonic structures allows detection of both increase and decrease of the amount the ammonia. Exposure time 1s. Related to Figure 4.

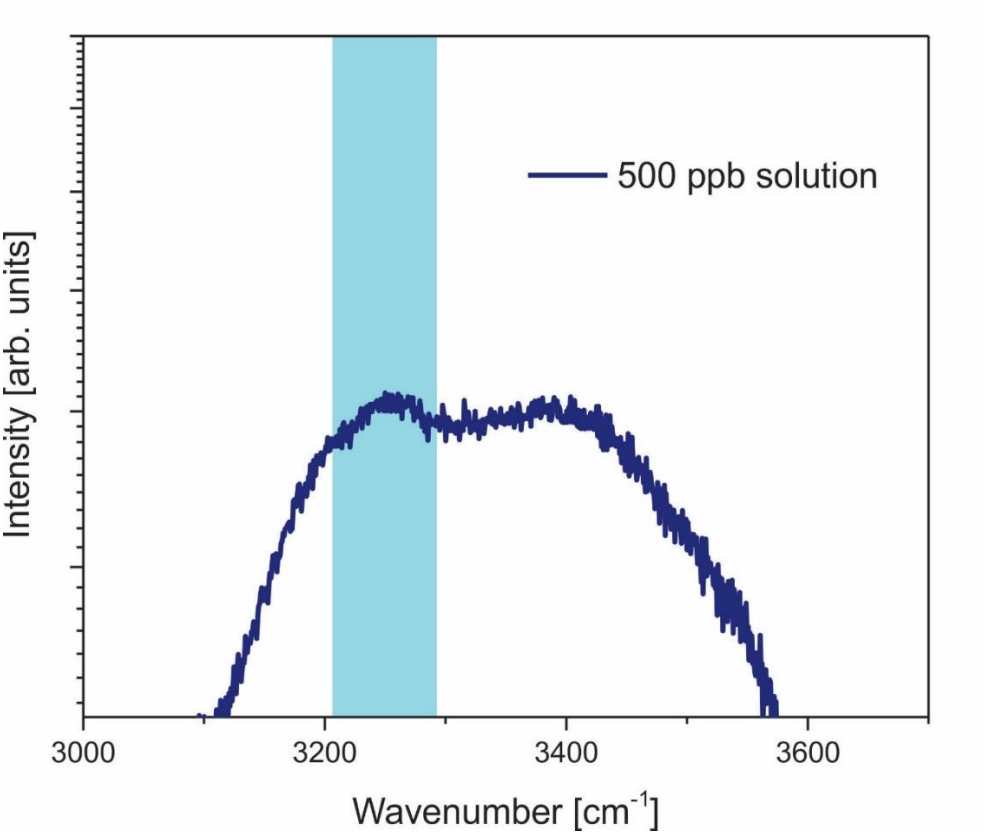

Figure SF6. Detection of 500 ppb ammonia concentration in aqueous solution on Ag plasmonic structures. Exposure time 1s. Related to Figure 5.

Table SF3. Conversion table. Simple approximation of amount of molecule in confocal volume. Related to Figure 4 and Figure 5.

p.p.b.	p.p.m.	mg/L	mmol/L	Number of molecules
50	0.05	2.936	5*10-6	3106
100	0.1	5.872	1*10-5	6212
500	0.5	29.358	5*10-5	31062
1000	1	58.717	1*10-4	62124
2000	2	117.433	2*10-4	124249

Transparent Methods

Solution preparation and pH measurement. Samples of ammonia solutions were prepared by diluting 56 wt% ammonium hydroxide ($NH_3 \cdot H_2O$) solution (VWR) with *Millipore* water. As results, concentrations of 0.1 ppm, 0.5 ppm, 1 ppm, 3 ppm, 5 ppm, 10 ppm, 20 ppm, 50 ppm, 100 ppm, 200 ppm, 500 ppm, 1000 ppm and 0.3 wt% (30, 000 ppm) ammonia solutions were made, based on the weight of NH_3 monomer and H_2O molecules.

In order to estimate the ratio of ammonia molecule (NH_3) and ammonium ions (NH_4^+), the pH values of ammonia solutions were measured. Specifically, the pH of pure Millipore water was measured at ~6.6 due to slight dissolving of ambient carbon dioxide. The pH values of 0.1 ppm, 10 ppm and 500 ppm solution were 10.7, 10.2 and 11.1 respectively. The NH_3/ NH_4^+ ratio was simply estimated by the acidity of ammonium (pKa = 9.25), according to:

$$\log_{10}(NH_3/NH_4^+) = \mathrm{pH} - \mathrm{pKa}$$

As results, the ammonia molecule (NH_3) content of all dilute ammonia samples were above 95 %, as compared to ammonium ions (NH_4^+).

Density Function Theory calculation. The calculation of vibrational modes and Raman intensities were performed using Gaussian09 quantum chemistry program(M. J. Frisch, 2010) at the M06-2X/aug-cc-pVTZ level of theory(Zhao and Truhlar, 2008). The structures of the ammonia molecule, ammonium ion, ammonia-ammonia dimer and ammonia-water complex were first optimized using tight convergence criteria and ultrafine integration grid after which the harmonic frequencies were calculated. To account for the anharmonic effects, which influence the frequencies of the stretching modes the most, anharmonic frequencies of the stretching modes were calculated using numerical differentiation along corresponding vibrational modes as implemented in the Gaussian09 software. To study the change in the Raman spectra of the ammonia molecule

and ammonia-water dimer due to the solvation, we also tested a model of fully solvated ammonia. The model was built by solvating ammonia-water dimmer with additional 12 water molecules after which the system was optimized. The number of water molecules was chosen to create a cluster in which ammonia-water dimmer would be fully surrounded by water molecules.

Plasmonic structures. Commercial SERS substrates SERStrate (Silmeco, Denmark) has been used. Substrates are based on leaned Si nanopillars covered with Ag resulting in resonance around 550 nm. Substrates structure was leaned using depositing of drop of nanopure water and drying it. The following procedure is done per vendor recommendation to increase interaction surface and enhancement effect.(Schmidt et al., 2012) For custom made silver nanoparticle SERS substrate commercially available Ag ink (Sigma Aldrich) has been used. The ink comprises silver nanoparticles of about 100 nm size and is pre-characterized by the vendor using optical and electron microscopy approaches. The film was deposited on a flat mica substrate, dried for 1 hour before use. SEM images of the resultant substrate layer were taken to confirm film morphology and particle size.

Raman microscopy. Raman experiments has been performed on custom modified Renishaw InVia Raman microscope. 532 nm SSDP laser was used as excitation source. All excitation and collection of Rama signal were done using 60x, 1.2NA water immersion objective (Olympus). For wide-field imaging beam was focused on input aperture of objective and slit opened to 100 μm size, corresponding to increase of spectral resolution to 9 cm^{-1}. For confocal experiments 1.5 mW at 532 nm has been used at the sample. For wide-field images 30 mW has been used to compensate change of the energy flux.

References

M. J. Frisch, G. W. T., H. B. Schlegel, G. E. Scuseria, M. A. Robb, J. R. Cheeseman, G. Scalmani, V. Barone, B. Mennucci, G. A. Petersson, H. Nakatsuji, M. Caricato, X. Li, H. P. Hratchian, A. F. Izmaylov, J. Bloino, G. Zheng, J. L. Sonnenberg, M. Hada, M. Ehara, K. Toyota, R. Fukuda, J. Hasegawa, M. Ishida, T. Nakajima, Y. Honda, O. Kitao, H. Nakai, T. Vreven, J. A. Montgomery, Jr., J. E. Peralta, F. Ogliaro, M. Bearpark, J. J. Heyd, E. Brothers, K. N. Kudin, V. N. Staroverov, T. Keith, R. Kobayashi, J. Normand, K. Raghavachari, A. Rendell, J. C. Burant, S. S. Iyengar, J. Tomasi, M. Cossi, N. Rega, J. M. Millam, M. Klene, J. E. Knox, J. B. Cross, V. Bakken, C. Adamo, J. Jaramillo, R. Gomperts, R. E. Stratmann, O. Yazyev, A. J. Austin, R. Cammi, C. Pomelli, J. W. Ochterski, R. L. Martin, K. Morokuma, V. G. Zakrzewski, G. A. Voth, P. Salvador, J. J. Dannenberg, S. Dapprich, A. D. Daniels, O. Farkas, J. B. Foresman, J. V. Ortiz, J. Cioslowski, and D. J. Fox (2010) 'Gaussian 09'.

Schmidt, M. S., Hübner, J. and Boisen, A. (2012) 'Large Area Fabrication of Leaning Silicon Nanopillars for Surface Enhanced Raman Spectroscopy', *Advanced Materials,* 24(10), pp. OP11-OP18.

Zhao, Y. and Truhlar, D. G. (2008) 'The M06 suite of density functionals for main group thermochemistry, thermochemical kinetics, noncovalent interactions, excited states, and transition elements: two new functionals and systematic testing of four M06-class functionals and 12 other functionals', *Theoretical Chemistry Accounts,* 120(1), pp. 215-241.